Biophysical Journal Volume 71 December 1996 3477–3487

Ryanodine Receptor Adaptation and Ca^{2+}-Induced Ca^{2+} Release–Dependent Ca^{2+} Oscillations

Joel Keizer*# and Leslie Levine*
*Institute of Theoretical Dynamics and #Section on Neurobiology, Physiology and Behavior, University of California, Davis, California 95616 USA

ABSTRACT A simplified mechanism that mimics "adaptation" of the ryanodine receptor (RyR) has been developed and its significance for Ca^{2+}-induced Ca^{2+} release and Ca^{2+} oscillations investigated. For parameters that reproduce experimental data for the RyR from cardiac cells, adaptation of the RyR in combination with sarco/endoplasmic reticulum Ca^{2+} ATPase Ca^{2+} pumps in the internal stores can give rise to either low $[Ca_i^{2+}]$ steady states or Ca^{2+} oscillations coexisting with unphysiologically high $[Ca_i^{2+}]$ steady states. In this closed-cell-type model rapid, adaptation-dependent Ca^{2+} oscillations occur only in limited ranges of parameters. In the presence of Ca^{2+} influx and efflux from outside the cell (open-cell model) Ca^{2+} oscillations occur for a wide range of physiological parameter values and have a period that is determined by the rate of Ca^{2+} refilling of the stores. Although the rate of adaptation of the RyR has a role in determining the shape and the period of the Ca^{2+} spike, it is not essential for their existence. This is in marked contrast with what is observed for the inositol 1,4,5-trisphosphate receptor for which the biphasic activation and inhibition of its activity by Ca^{2+} are sufficient to produce oscillations. Results for this model are compared with those based on Ca^{2+}-induced Ca^{2+} release alone in the bullfrog sympathetic neuron. This kinetic model should be suitable for analyzing phenomena associated with "Ca^{2+} sparks," including their merger into Ca^{2+} waves in cardiac myocytes.

INTRODUCTION

In a recent series of papers Fill and co-workers (Györke and Fill, 1993; Györke and Fill, 1994; Györke et al., 1994; Louis, 1994) have shown that the ryanodine receptor (RyR) from cardiac cells and skeletal muscle undergoes a Ca^{2+}-dependent process called "adaptation." Adaptation occurs during the slow, spontaneous decrease in the open probability of a channel after it has been activated rapidly by a sustained pulse of Ca^{2+} at its cytosolic face ($[Ca_i^{2+}]$). In isolated bilayers, activation of the RyR occurs within milliseconds, whereas inactivation occurs on a time scale of a few seconds. The RyR is said to have "adapted" during inactivation because a subsequent increase in $[Ca_i^{2+}]$ produces a nearly identical rise in the open probability. The extent of opening just after Ca^{2+} stimulation (the peak open probability) and that after inactivation (the plateau) both increase with increasing Ca^{2+} concentration. In cardiac cells the plateau open probability does not exhibit further inactivation until millimolar Ca^{2+} concentrations are reached (Chu et al., 1993; Laver et al., 1995). Although RyRs from skeletal muscle (Laver et al., 1995) and brain (Bezprozvanny et al., 1991) are more sensitive to inactivation by Ca^{2+}, they do not exhibit significant inactivation below ~0.1 mM $[Ca_i^{2+}]$. Thus Ca^{2+} release via the RyR appears to be dominated by fast Ca^{2+} activation followed by slower inactivation to the plateau in the physiological range of $[Ca_i^{2+}]$.

This process of adaptation is reminiscent of the Ca^{2+} release properties of the inositol 1,4,5-trisphosphate (IP_3) receptor Ca^{2+} channel (IP_3R) (Iino, 1990). The IP_3R also undergoes rapid Ca^{2+}-dependent activation followed by a slow inactivation. For the IP_3R, however, inactivation is known to be Ca^{2+} dependent, although it also occurs on a time scale of seconds (Iino, 1990; Bezprozvanny et al., 1991; Finch et al., 1991). This type of ligand-gated regulation of ion channel is analogous to the rapid voltage-dependent activation and inactivation of sodium channels, and these properties of the IP_3R give it a similar role in the Ca^{2+} excitability of the endoplasmic reticulum (ER) membrane (Li et al., 1995).

Structural similarities between the RyR and the IP_3R (Berridge, 1993) might suggest that the mechanisms underlying Ca^{2+} release may be similar. This correspondence, however, cannot be strictly true because in the physiological range of $[Ca_i^{2+}]$ the equilibrium (plateau) open probability of the IP_3R is a bell-shaped, rather than an increasing, function of $[Ca_i^{2+}]$. Inactivation of the IP_3R dominates above ~0.3 μM (Bezprozvanny et al., 1991; Iino and Tsukioka, 1994). This bell-shaped Ca^{2+} dependence of the IP_3R along with slow inactivation by Ca^{2+} has been proposed to have an important role in IP_3-induced Ca^{2+} oscillations (De Young and Keizer, 1992) and used to explain the complex pattern of Ca^{2+} oscillations in pituitary gonadotrophs (Keizer et al., 1995).

Here we develop a simplified model of the regulation of the RyR by $[Ca_i^{2+}]$ that reproduces semiquantitatively the gross observations of adaptation. The present model correctly predicts a nondiminishing equilibrium open probabil

Received for publication 25 March 1996 and in final form 6 September 1996.

Address reprints to Dr. Joel E. Keizer, Institute of Theoretical Dynamics, University of California, Davis, CA 95616-8618. Tel.: 916-752-0938; Fax: 916-752-7297; E-mail: jekeizer@ucdavis.edu.

0006-3495/96/12/3477/11 $2.00

ity when $[Ca_i^{2+}]$ is in the range 0.1–100 μM. We term the model "simplified" because not enough detail is yet known about the kinetics of the RyR to permit us to establish a definite molecular mechanism. Our mechanism for adaptation differs from other proposed mechanisms (Tang and Othmer, 1994; Cheng et al., 1995; Sachs et al., 1995) in that Ca^{2+} is not directly involved in inactivation. We translate our mechanism of adaptation into differential equations, which we analyze by using the difference in the activation and adaptation time scales.

Our motivation for developing the kinetic equations is twofold. First, we were curious about how regulation of the RyR at physiological concentrations of Ca^{2+} compared with that of the IP_3R. As we show in what follows, the minimal mechanism developed here differs substantially from that by which $[Ca_i^{2+}]$ activates and inactivates the IP_3R (De Young and Keizer, 1992). Second, we wanted to explore the role of adaptation in Ca^{2+} oscillations (Friel and Tsien, 1992; Cheng et al., 1996). In the absence of external Ca^{2+} fluxes (closed-cell model) the mechanism leads to bistability, i.e., more than one steady state or oscillation occurring for a given set of parameters. Simulations show for a variety of realistic parameters that at one of these steady states $[Ca_i^{2+}]$ is well above the physiological range. Thus we also investigate the influence of external Ca^{2+} fluxes (open-cell model). Physiological values of Ca^{2+} influx and efflux give rise to much slower Ca^{2+} oscillations, similar to the caffeine-sensitive oscillations found in the bullfrog sympathetic neuron (Friel and Tsien, 1992). Adaptation of the RyR helps to determine the shape and the period, but not the existence, of Ca^{2+} spikes. These external flux-dependent oscillations require only Ca^{2+}-induced Ca^{2+} release (CICR) and involve emptying and refilling of internal stores. Finally we compare our results with those of other mechanisms, including those involving CICR (Tang and Othmer, 1994; Friel, 1995) and IP_3-induced Ca^{2+} release (IICR) (De Young and Keizer, 1992; Keizer et al., 1995; Li et al., 1995).

ADAPTATION OF THE RyR

The mechanism used to mimic adaptation of the RyR is shown schematically in Fig. 1. States C_1 and C_2 are closed states, with state C_1 dominating at low $[Ca_i^{2+}]$. States O_1 and O_2 are open states. For simplicity we have taken these states to be states of the entire RyR rather than states of the four (possibly interacting) subunits, because little is known about how the subunits function (Ogawa, 1994). Transitions from C_1 to O_1 and from O_1 to O_2 are assumed to be Ca^{2+} dependent and have been written as depending on the binding of n and m Ca^{2+} ions, respectively. These steps correspond to the phenomenon of CICR and in the absence of the transition from O_1 to C_2 the mechanism would not give rise to adaptation. When the transitions between O_1 and C_2 are sufficiently slow, the mechanism exhibits slow inactivation and, as we show in what follows, adaptation. We note that

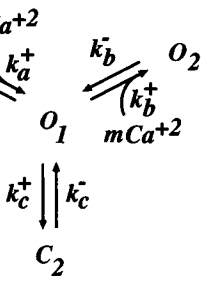

FIGURE 1 Schematic diagram of transitions among the four states of the RyR used to describe adaptation. States C_1 and C_2 are closed states, and O_1 and O_2 are open states, assumed to have the same single-channel conductance. The k are rate constants; only steps a and b are Ca^{2+} dependent.

the second open state, O_2, is an important part of the model that is required to keep the plateau open probability (see below) increasing as $[Ca_i^{2+}]$ is increased.

To analyze the mechanism in Fig. 1 we translate the schematic diagram into kinetic equations, using the mass action law. Although multiple Ca^{2+} ions certainly do not bind simultaneously to the RyR, for n and m greater than 1 we have in mind the Hill-type approximation often used for multimeric proteins. Adopting the notation that P_{C_1} gives the fraction of RyR that is in the state C_1, etc. gives the following set of differential equations:

$$dP_{C_1}/dt = -k_a^+[Ca_i^{2+}]_i^n P_{C_1} + k_a^- P_{O_1}, \tag{1}$$

$$dP_{O_1}/dt = k_a^+[Ca_i^{2+}]_i^n P_{C_1} - k_a^- P_{O_1} - k_b^+[Ca_i^{2+}]_i^m P_{O_1} + k_b^- P_{O_2} - k_c^+ P_{O_1} + k_c^- P_{C_2}, \tag{2}$$

$$dP_{O_2}/dt = k_b^+[Ca_i^{2+}]_i^m P_{O_1} - k_b^- P_{O_2}, \tag{3}$$

$$dP_{C_2}/dt = k_c^+ P_{O_1} - k_c^- P_{C_2}, \tag{4}$$

where the subscripts a, b, and c label the three kinetic steps in Fig. 1. The $k_i^{\pm}$ are rate constants, which along with the integers n and m are to be determined by data fitting. Qualitatively steps a and b should be fast (millisecond time scale), whereas step c should be slow (second time scale). Using the condition $P_{C_1} + P_{C_2} + P_{O_1} + P_{O_2} = 1$, we can eliminate one of these equations, yielding three independent equations. When $[Ca_i^{2+}]$ is held fixed, these three equations are linear and straightforward to analyze.

To fix the kinetic parameters of the model we have relied on the data of Györke and Fill (1993) on the time course of the open probability following step increases in $[Ca_i^{2+}]$ from 0.1 μM for the cardiac RyR. Key features of these data include rapid activation to the peak, the dependence of the peak open probability on $[Ca_i^{2+}]$, the slow decline to the plateau, and the $[Ca_i^{2+}]$ dependence of the plateau open probability. Values of the kinetic parameter that produce a semiquantitative fit with experiment are given in Table 1. Figure 2 *A* shows a simulation of the open probability, $P_O = P_{O_1} + P_{O_2}$, for an instantaneous increase of $[Ca_i^{2+}]$ from 0.1 to 0.9 μM. The initial rise to the peak occurs on the millisecond time scale (cf. Appendix A), whereas the de

TABLE 1 RyR kinetic constants ($n = 4$, $m = 3$)

Rate constant	Value
k_a^+	1500 μM^{-4} s^{-1}
k_a^-	28.8 s^{-1}
k_b^+	1500 μM^{-3} s^{-1}
k_b^-	385.9 s^{-1}
k_c^+	1.75 s^{-1}
k_c^-	0.1 s^{-1}

cline to the plateau (Fig. 2 *B*) occurs within a few seconds. With these parameters the model also mimics "adaptation," as is shown in Fig. 2 *C*, where a further increase of $[Ca_i^{2+}]$ to 0.50 μM at the arrow gives rise to a comparable peak in P_O.

It is easy to see how the features of the kinetic model give rise to rapid activation, slow inactivation, and "adaptation." Referring to Fig. 1, we see that at low $[Ca^{2+}]$ the RyR will occupy predominantly the closed state, C_1. In fact, at a basal concentration of 0.1 μM the open probability is ~0.01 in our model. A rapid jump in $[Ca^{2+}]$ from 0.1 to 0.9 μM (as in Fig. 2 *A*) increases the occupancy of the two open states within milliseconds because of the rapid Ca^{2+} dependence of the transitions in steps *a* and *b*. This leads to the peak open probability, which is followed by a decline as the rapidly equilibrating transitions in steps *a* and *b* slowly lose occupancy owing to the slow transition *c* to state C_2. Adaptation, as illustrated in Fig. 2 *C*, occurs before complete equilibration of step *c* and is due to the residual occupancy of the closed state, C_1 of the RyR, which can be recruited into the open states by a second pulse of Ca^{2+}.

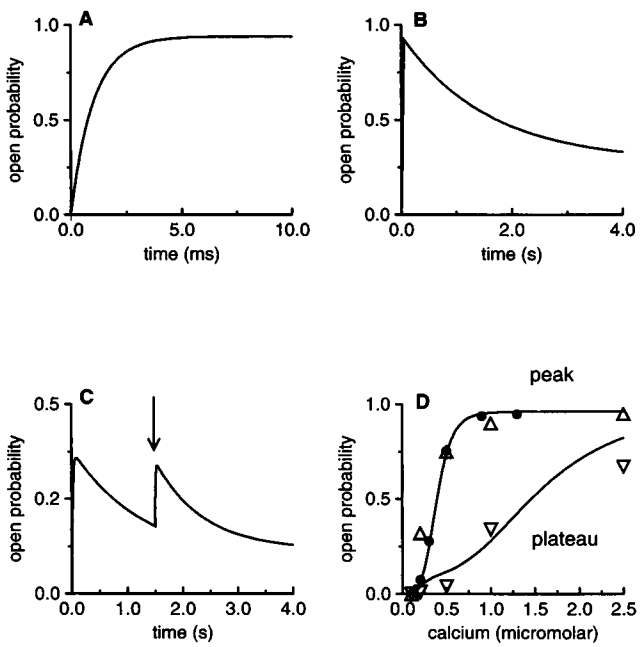

FIGURE 2 (*A*) Simulation of the rapid rise to the peak open probability of a single RyR following an increase of $[Ca_i^{2+}]$ from 0.1 to 0.9 μM, calculated with Eqs. 1–4 and the rate constants in Table 1. (*B*) Same as (*A*) but on a longer time scale to show the decline to the plateau open probability. (*C*) Same as (*B*) but with two increases in $[Ca_i^{2+}]$: from 0.1 to 0.35 μM at $t = 0$ followed by an increase to 0.50 μM at the arrow. Note the adapted response. (*D*) The peak and the plateau open probabilities as functions of $[Ca_i^{2+}]$. (*Solid curves*) Theoretical values from Eqs. 15 and 16; (●) simulations like that in (*A*); (△) Experimental data (Fig. 2 *B* of Györke and Fill, 1993) (upward facing triangles are the peak; and downward, the plateau).

The dependence of the peak and plateau responses for increases in $[Ca_i^{2+}]$ from 0.1 μM to higher values is shown in Fig. 2 *D*. The filled circles represent the peak values taken from simulations like that in Fig. 2 *A*, whereas the curves are theoretical values based on the separation of the "fast" time scale for the rise to the peak (milliseconds) from the "slow" time scale for the decline to the plateau (seconds). The derivation of these theoretical expressions is given in Appendix A. The calculated values for P_O^{peak} are in good agreement with the experimental results of Györke and Fill (1993) (shown as the open triangles). This includes the facts that P_O saturates slightly below $P_0 = 1$ (0.963 in Fig. 2 *A*) and that P_O is negligible for $[Ca_i^{2+}] \leq 0.1$ μM (Fig. 2 *D*). At values of $[Ca_i^{2+}]$ higher than 5 μM the plateau, on the other hand, rises somewhat higher (1.0 rather than 0.75) than is reported experimentally. This problem can be remedied in the model by addition of another closed state, C_3, that is connected to C_2 by a $[Ca_i^{2+}]$-dependent transition. For the sake of simplicity, however, and because the difference is significant only when $[Ca_i^{2+}]$ is at the high end of the physiological range (Alberts et al., 1989), we have not included that additional kinetic step in the version of the model presented here.

On a time scale longer than 10–20 ms it is possible to approximate the values of P_{C_1}, P_{O_1}, and P_{O_2} by taking advantage of the fact that the kinetic steps *a* and *b* in Fig. 1 rapidly reach equilibrium before P_{C_2} changes appreciably. On the "slow" time scale of changes in P_{C_2} it is shown in Appendix B that the open probability can be approximated by

$$P_O^{slow} = \frac{w(1 + ([Ca_i^{2+}]/K_b)^3)}{1 + (K_a/[Ca_i^{2+}])^4 + ([Ca_i^{2+}]/K_b)^3}, \quad (5)$$

where $w = 1 - P_{C_2}$, the fraction of channels not in state C_2. Furthermore, on this time scale w solves the differential equation

$$dw/dt = -(w - w^\infty([Ca_i^{2+}]))/\tau([Ca_i^{2+}]), \quad (6)$$

where w^∞ is the equilibrium value of w and τ is its relaxation time. Explicit expressions for $w^\infty([Ca_i^{2+}])$ and $\tau([Ca_i^{2+}])$ are given in Eqs. 20 and 21 in Appendix B.

For fixed values of $[Ca_i^{2+}]$, Eqs. 5 and 6 show that the rate of relaxation of w determines the rate of relaxation of P_O to its plateau value in Fig. 2 *D*. In the model the relaxation time depends on $[Ca_i^{2+}]$ and has a value of 1.0 s for $[Ca_i^{2+}] = 0.5$ μM. For the parameter values in Table 1 the relaxation time increases to ~2.0 s at $[Ca_i^{2+}] = 0.2$ μM and to ~1.9 s at $[Ca_i^{2+}] = 1.0$ μM. This is compatible with the experimental relaxation time of 1.3 ± 0.3 s reported for the cardiac RyR (Györke and Fill, 1993).

Although this minimal model does a good job of reproducing experiments on adaptation of the RyR, we would not expect stochastic simulations with the model to reproduce all the detailed transitions observed in single-channel currents. We have verified, however, that the gross features of the single-channels currents observed by Györke and Fill (1993) are reproduced. These include periods of sustained opening with brief interruptions to state C_1 followed by periods of sustained closings in which the channel is in state C_2. What is missing are the rapid "flickerings" of the channel in the open state. Reproducing that and other features seen in the single-channel records would require a more detailed model. Nonetheless, an ensemble average of simulations with the present model is guaranteed to duplicate the results in Fig. 2.

ADAPTATION IMPLIES BISTABLE $[Ca_i^{2+}]$ IN A CLOSED CELL

Fast activation of the IP_3R by $[Ca_i^{2+}]$ followed by slow inactivation by $[Ca_i^{2+}]$ is sufficient to explain IP_3-induced $[Ca_i^{2+}]$ oscillations in a number of cells types (De Young and Keizer, 1992; Atri et al., 1993; Keizer et al., 1995). Those oscillations can occur in the absence of Ca^{2+} influx and efflux. To test whether adaptation of the RyR, which also involves coordinated fast $[Ca_i^{2+}]$ activation and slow inactivation, might also cause oscillations in Ca^{2+}, we have explored a closed-cell kinetic model. Here we use our kinetic model of the RyR to describe CICR from an internal store (ER or sarcoplasmic reticulum). This is combined with a passive leak and a sarco/endoplasmic reticulum Ca^{2+} ATPase– (SERCA-) type pump (Lytton et al., 1992) that returns Ca^{2+} to the store. With the separation between fast and slow time scales described in the previous section, the differential equations for the closed-cell model are the balance equation for $[Ca_i^{2+}]$ and the relaxation equation for w, i.e.,

$$d[Ca_i^{2+}]/dt \tag{7}$$

$$= f_i\left((v_1 P_0^{slow} + v_2)([Ca_s^{2+}] - [Ca_i^{2+}]) - v_3\frac{[Ca_i^{2+}]^2}{[Ca_i^{2+}]^2 + K_3^2}\right),$$

$$dw/dt = -(w - w^{\infty}([Ca_i^{2+}]))/\tau([Ca_i^{2+}]) \tag{8}$$

where f_i is the fraction of Ca^{2+} that is unbound (free) in the cytoplasm and $[Ca_s^{2+}]$ is the Ca^{2+} concentration in the store. Because the cell is assumed to be closed to Ca^{2+} influx and efflux,

$$[Ca_s^{2+}] = (C_o - [Ca_i^{2+}])(V_i f_s/V_s f_i) = (C_o - [Ca_i^{2+}])/c_1, \tag{9}$$

where V_i and V_s are the volumes of the cytoplasm and the internal store, respectively, f_s is the buffering factor for the store, and $C_o V_i$ is the total amount of free Ca^{2+} in the cell. The factor c_1 is sometimes referred to as the ratio of the effective volume of the store to that of the cytoplasm (Friel, 1995). The three terms on the right-hand side of Eq. 7 are contributions to the Ca^{2+} balance in the cytoplasm that come from the RyR, the leak, and the SERCA pump, respectively.

Equation 7 introduces seven new parameters, three of which can be given approximate values based on experiment: $f_i = 0.01$ (Tse et al., 1994a), $c_1 = 0.15$ (Alberts et al., 1989), and $K_3 = 0.3$ μM (Lytton et al., 1992). The steady states of these equations depend, however, only on the two ratios v_2/v_1 and v_3/v_1 and C_o. These parameters can be partially fixed by the requirement that steady-state values of $[Ca_i^{2+}]$ and $[Ca_s^{2+}]$ fall in the physiological range (orders) of 0.05–0.10 μM (Alberts et al., 1989) and 50–150 μM (Hofer and Machen, 1994; Tse et al., 1994b), respectively). A further restriction comes from the fact that Ca^{2+} oscillations generally occur with periods in the range 2–200 s (Berridge and Galione, 1988). Thus a rather restricted range of these four parameters determines whether Ca^{2+} oscillations can occur. For simplicity and to restrict the parameters further, we take $v_1 = 40\ s^{-1}$, which is a compromise between those estimated in Friel's analysis of the bullfrog sympathetic neuron (Friel, 1995).

For reference a standard set of values for the parameters is given in Table 2. These parameters correspond to steady-state values of $[Ca_i^{2+}]$ and $[Ca_s^{2+}]$ of 0.056 and 66.3 μM, respectively, both in the physiological range. Table 2 also provides an alternative set of rate parameters, indicated in parentheses. Those rate parameters are smaller and correspond to an internal store with a small effective volume ($c_1 = 0.02$). The steady-state values of $[Ca_i^{2+}]$ and $[Ca_s^{2+}]$ for the alternative rates are 0.095 and 55 μM. For simplicity, we refer to the standard set of parameters as representing a large internal store and the alternative set as representing a small internal store. Although in many cells either the ER or the sarcoplasmic reticulum occupies 10–20% of the cytosolic volume (Alberts et al., 1989), this is not the case in all cells. For example, resting T-lymphocytes have an extremely small ER. To account for this diversity, we simulate whole cells with both small and large internal stores.

TABLE 2 Parameters for the closed-cell model

Parameter	Value	Meaning/Equation
f_i	0.01	Buffer factor in cytoplasm/Eq. 7
v_1	40 s^{-1} (5 s^{-1})	Rate constant for RyR/ Eq. 7
v_2	0.5 s^{-1} (0.15 s^{-1})	Rate constant for store leak/Eq. 7
v_3	1000 μM s^{-1} (100 μM s^{-1})	Maximal rate of SERCA pump/Eq. 7
k_3	0.30 μM	Dissociation constant for SERCA/Eq. 7
$c_1 = V_s f_i/V_i f_s$	0.15 (0.02)	Weighted volume fraction/Eq. 9
C_o	10 μM (1.2 μM)	Total $[Ca^{2+}]$ in cell/Eq. 9

Small-store parameters are given in parentheses.

Both the large-store and the small-store closed cells exhibit bistability, i.e., the coexistence of several steady or oscillatory states. Figure 3 illustrates this situation for a large store by plotting the steady values of $[Ca_i^{2+}]$ that are possible as a function of the total free-calcium concentration, C_o. At low values of C_o, only a single, stable value of $[Ca_i^{2+}]$ is possible. This is shown by the solid curve. However, for values of C_o between ~7.5 and 27 μM, three or more steady states are possible. The high steady-state branch (*solid curve*) is stable, whereas the branch or branches at intermediate values of $[Ca_i^{2+}]$ are unstable (*dashed curve*). This model even exhibits oscillatory states near C_o = 27 μM (*open diamond*). However, those oscillations are unstable and are not relevant physiologically. The bistability illustrated in Fig. 3 is typical of what we find for other variations of the large-store parameter set, although for some parameter changes, viz., v_2 = 0.05 s^{-1}, v_3 = 1200 $\mu M\ s^{-1}$, and C_o = 13 μM, stable oscillations of small amplitude occur. Nonetheless, in every case in which a stable oscillation is observed, both the range of parameters that support oscillations is small and the oscillations coexist with an unphysiologically high steady state of $[Ca_i^{2+}]$ (2 μM and above) that is stable. Those oscillations are crucially dependent on slow adaptation of the RyR and have periods in the range of 2–6 s.

Figure 4 shows that the small-store model of a closed cell also exhibits bistability but with a more complex stucture. Again the steady states at low values of C_o are stable (*solid curve, left*), but for C_o in two separate ranges of values stable steady oscillations exist. This figure is called a bifurcation diagram and provides a compact summary of the dynamic behavior of $[Ca_i^{2+}]$ as the total free-Ca^{2+} concentration, C_o, is varied. Rather than showing the time dependence of oscillations for a particular value of C_o, Fig. 4 shows the maximum and minimum values of $[Ca_i^{2+}]$ in these oscillations as a function of C_o. The stable oscillations

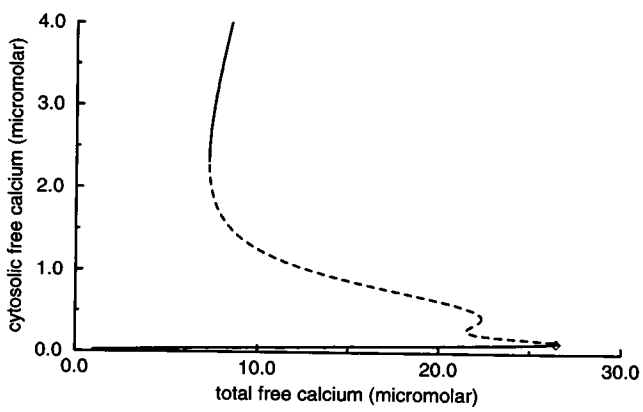

FIGURE 3 Bifurcation diagram of the steady and the oscillatory states of cytosolic free Ca^{2+} as a function of total free-calcium concentration, C_o. Calculated with the large-store, closed-cell model parameters in Table 2. (*Solid curves*) Stable steady states, (*dashed curve*) unstable states. (◇) Location of a small-amplitude, unstable oscillation. This figure and Figs. 4–9 were calculated using Xppaut (Ermentrout, 1995).

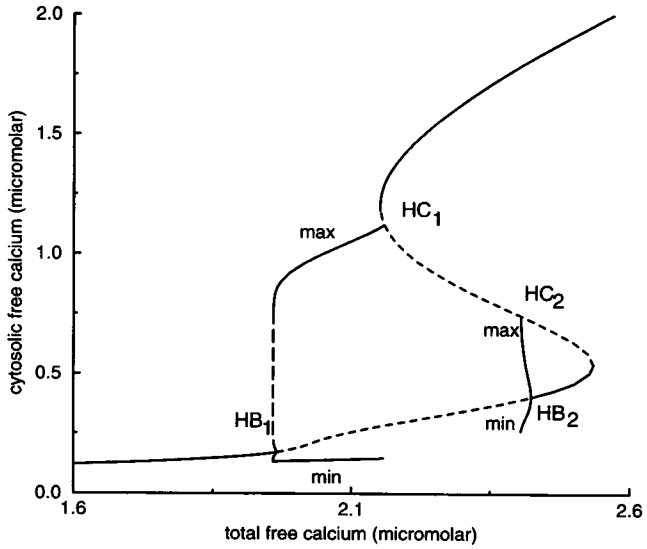

FIGURE 4 Same as Fig. 2, except for the small-store parameters in Table 2: (— — — —) Unstable states; (———— *max*), (———— *min*) maximum and minimum values, respectively, of stable oscillations. HB_1 and HB_2 are Hopf bifurcation points, and HC_1 and HC_2 are homoclinic points. For certain values of the total free-calcium concentration several stable steady or oscillatory states are possible.

are indicated by the solid curves labeled max and min, and unstable states are indicated with dashed curves. For values of C_o between the points labeled HB_1 = 1.97 and HC_1 = 2.17 μM the oscillations are stable, with periods of the order of 20 s. Near the point labeled HB_2 = 2.42 μM, smaller amplitude oscillations coexist with a branch of high $[Ca_i^{2+}]$ steady states. These oscillatory regimes terminate at points HC_1 and HC_2, where the oscillations intersect the central branch of unstable steady states (*dashed curves*).

From these and other simulations we conclude that stable oscillations based on the inactivation kinetics of the RyR can occur under special circumstances in a closed cell. These oscillations, however, invariably coexist or are closely associated with stable steady states that have unphysiologically high values of $[Ca_i^{2+}]$. Indeed, we have explored a large variation for all the parameters in Table 2 and find that in the physiological range our simulations give rise to results similar to those in Figs. 3 and 4. Thus, unlike the comparable situation for the IP_3R (Keizer et al., 1995), these oscillations are unlikely to be relevant physiologically.

CICR, NOT ADAPTATION, PRODUCES OSCILLATIONS IN OPEN CELLS

All cells have mechanisms for controlling influx and efflux of Ca^{2+} from the external medium (Scharff and Foder, 1993) and are, therefore, "open." The simplest type of open cell contains voltage-activated Ca^{2+} channels for which one can fix the rate of influx by clamping the plasma membrane potential (Hille, 1992). To mimic this situation we consider an open-cell model with a constant influx of external Ca^{2+}, j_{in}, that can be controlled parametrically. Although both

Ca^{2+} pumps and exchange mechanisms are prevalent in the plasma membrane of cells, we treat efflux as occurring via a plasma membrane Ca^{2+}-ATPase (PMCA pump) only (Carafoli, 1994). Adding these terms to the closed-cell model described in the previous section gives the open-cell $[Ca_i^{2+}]$ balance equation:

$$d[Ca_i^{2+}]/dt = f_i\Big((v_1 P_O^{slow} + v_2)([Ca_s^{2+}] - [Ca_i^{2+}]) - v_3\frac{[Ca_i^{2+}]^2}{[Ca_i^{2+}]^2 + K_3^2} - v_{out}\frac{[Ca_i^{2+}]^2}{[Ca_i^{2+}]^2 + K_{out}^2} + j_{in}\Big), \quad (10)$$

where the final two terms represent the PMCA pump (Carafoli, 1994) and the Ca^{2+} influx. Because the cell is open to the external medium, the total free-Ca^{2+} concentration, C_o, is no longer fixed but varies according to the equation

$$dC_o/dt = f_i\Big(j_{in} - v_{out}\frac{[Ca_i^{2+}]^2}{[Ca_i^{2+}]^2 + K_{out}^2}\Big). \quad (11)$$

These two equations, along with Eq. 8 and the definitions of P_O^{slow} and $[Ca_s^{2+}]$ in Eqs. 5 and 9, describe how $[Ca_i^{2+}]$ responds to alterations in the rate of influx, j_{in}.

The open-cell model involves three new parameters: j_{in}, K_{out}, and v_{out}. Inasmuch as j_{in} represents influx from a clamped membrane potential in an electrically excitable cell, it can be estimated from whole-cell Ca^{2+} currents. A current of 0.1 pA in a cell with a volume of 1000 μm^3 gives a value of $j_{in} \simeq 1\ \mu M\ s^{-1}$, and we use values of j_{in} of this magnitude (see Table 3), which are similar to those measured in the bullfrog sympathetic neuron (Friel, 1995). The value of the dissociation contant, K_{out}, is known to be larger than that of the SERCA pump, and, based on measurements in Jurkat (R. Dolmesch and R. Lewis, personal communication) and red-blood cells (Carafoli, 1994), we take $K_{out} = 0.6\ \mu M$. The value of v_{out} also has been estimated in Jurkat cells (R. Dolmesch and R. Lewis, personal communication) and in pancreatic acinar cells (Tepikin et al., 1992) to be $\sim 10\ \mu M\ s^{-1}$. In combination with the maximal leak (v_2) and pump rates (v_3) for the internal stores, v_{out} determines the steady-state values of $[Ca_i^{2+}]$ and $[Ca_s^{2+}]$. We have required these to be of the order of 0.05–0.10 and 50–150 μM, respectively. In the open-cell model the maximal leak rate can be quite small, and it is set close to zero. Reference values for the additional parameters in the open-cell model are given in Table 3.

TABLE 3 Additional parameters for the open-cell model

Parameter	Value	Meaning/Equation
v_2	0.5 s^{-1} (0.1 s^{-1})	Maximal rate of store leak/Eq. 10
v_3	120 $\mu M\ s^{-1}$	Maximal rate of SERCA pump/Eq. 10
v_{out}	9.0 $\mu M\ s^{-1}$	Maximal rate of PMCA pump/Eq. 10
K_{out}	0.60 μM	Dissociation constant for PMCA/Eq. 10
j_{in}	1.0 $\mu M\ s^{-1}$	Constant influx rate/Eq. 10

Small-store parameters are given in parentheses.

Figure 5 illustrates the sorts of oscillation in $[Ca_i^{2+}]$ and $[Ca_s^{2+}]$ that occur with the open-cell model for the large-store and small-store parameters listed in Table 3. Despite the fact that the cell with a large store contains more total free Ca^{2+}, the actual free-Ca^{2+} concentration in the store, $[Ca_s^{2+}]$, is less than half of that of the cell with a small store. The larger total free-Ca^{2+} concentration for a large store is reflected in the larger amplitude of the oscillations in $[Ca_i^{2+}]$ and in a smaller-amplitude oscillation in $[Ca_s^{2+}]$. These oscillations are typical of what is observed with parameter values in the range of those in Table 3, with substantially larger amplitude oscillations observed when j_{in} and v_{out} are increased. Comparing the two parts of Fig. 5 shows that spikes in $[Ca_i^{2+}]$ are preceded by store refilling and occur simultaneously with rapid, partial depletion of the stores. This type of oscillation is completely dependent on the refilling of the stores through the influx term, j_{in}. Indeed, setting j_{in} to zero has the effect of eliminating all further spikes and, if it is done during the spiking phase, terminates the spike prematurely.

We have explored the influence of adaptation of the RyR on this type of fill-and-release Ca^{2+} oscillation by altering the rate at which adaptation occurs. The effect of making adaptation fast (decreasing τ in Eq. 21 by increasing k_c^- to 10 s^{-1}) is shown in Fig. 6. For both the large- and the small-store cases the amplitude, the shape, and the period—but not the existence—of the oscillations are modified. If

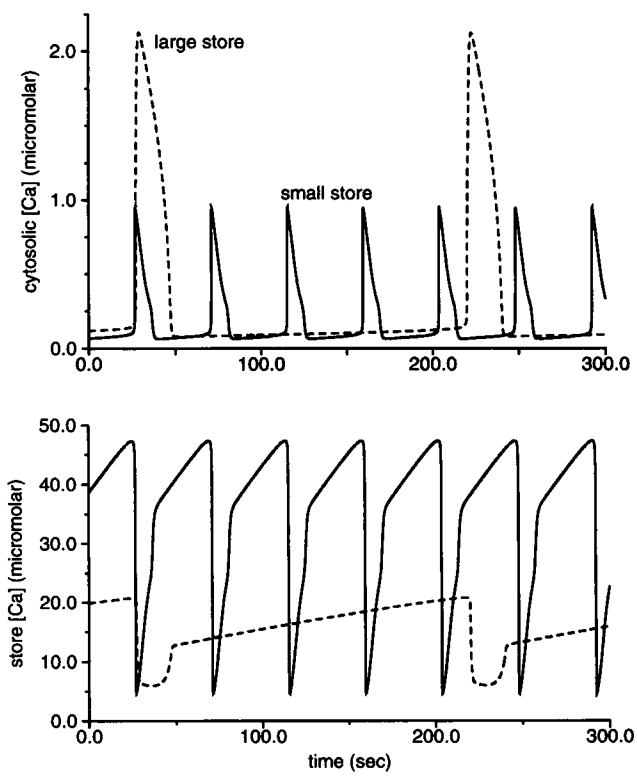

FIGURE 5 Oscillations in (*top*) $[Ca_i^{2+}]$ and (*bottom*) $[Ca_s^{2+}]$ for the open-cell model; (————) Small internal store, (— — — —) large internal store; other parameters are given in Table 3.

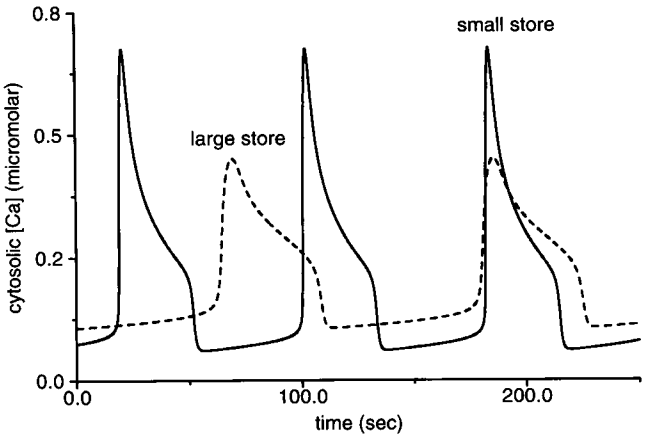

FIGURE 6 Oscillations in $[Ca_i^{2+}]$ for the open-cell model; same parameters as in Fig. 5, except that k_c^- is increased from 0.175 to 10.0 s^{-1}, speeding adaptation.

adaptation is made slower (k_c = 0.01 s^{-1}), oscillations also occur, but with an increased amplitude.

Adaptation involves a transition between the peak and plateau open responses of the RyR to increases in $[Ca_i^{2+}]$ (cf. Fig. 2 *D*), and Fig. 7 shows the open probability, P_O^{slow}, as a function of $[Ca_i^{2+}]$ for the small-store oscillations in Figs. 5 and 6. The arrows in Fig. 7 show the directions of time. For the experimental value k_c^- = 0.175 s^{-1} (*slow adaptation*) the open probability follows the peak curve on the upstroke of the spike and then declines toward the plateau curve on the slower downstroke. Increasing k_c^- to 10 s^{-1} (*fast adaptation*) has the effect of keeping the open probability close to the lower plateau curve on both the upstroke and the downstroke of the spike. Decreasing k_c^- by a similar factor restricts the spike to the peak open probability curve. Thus although adaptation plays a role in these oscillations, it is obviously not an essential feature in determining their existence. Thus it appears that CICR is a sufficient basis for RyR-based oscillations in the open cell, a conclusion that is reinforced by the simplified model in the next section.

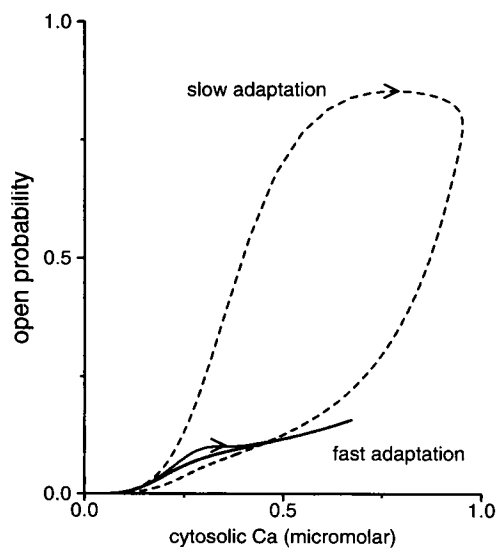

FIGURE 7 Open probability as a function of $[Ca_i^{2+}]$ during an oscillation for the open-cell model: (*slow adaptation*) the large store in Fig. 5 (0.175 s^{-1}), (*fast adaptation*) the large store in Fig. 6 (10.0 s^{-1}). (*Arrow*) Direction of change in time. With adaptation slow, the upstroke follows the peak open probability and the downstroke the plateau probability. With adaptation fast, both upstroke and downstroke follow the plateau.

SIMPLIFIED OPEN-CELL MODEL

The fact that adaptation is not essential for oscillations in the open-cell model suggests that one can simplify the model either by fixing the value of w near its initial value on the peak curve (0.963) or by requiring that

$$w = w^{\infty}([Ca_i^{2+}]). \tag{12}$$

The former simplification corresponds to adaptation that is considerably slower, and Eq. 12 to adaptation that is considerably faster, than in the experiments of Györke and Fill (1993). As there is evidence (Valdivia, et al., 1995) that adaptation occurs more rapidly in vivo than in vitro, we simplified the open-cell model, using Eq. 12. In this case the open probability always follows the adapted plateau curve.

In this simplified model, only $[Ca_i^{2+}]$ and C_o are variables, and the equations are analogous to those used by Friel to describe the bullfrog sympathetic neuron (Friel, 1995). As expected from the results in Fig. 6, the simplified model supports Ca^{2+} oscillations, although with a somewhat reduced amplitude. This is shown in Fig. 8, where the stable (*solid curves*) and the unstable (*short-dashed line*) steady states and the maximum (*max*) and the minimum (*min*) values of $[Ca_i^{2+}]$ during oscillations are shown as functions of the influx rate, j_{in}. Three features of these curves are

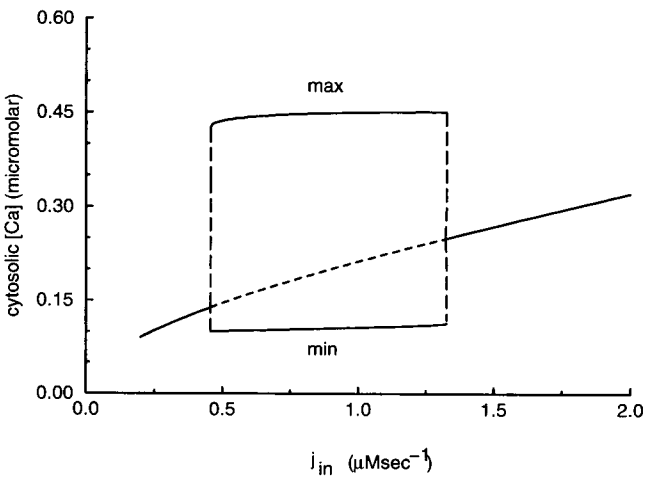

FIGURE 8 Bifurcation diagram for the simplified open-cell model. The stable steady states (—), the unstable steady states (– – – –), the unstable oscillations (— — — —), and the stable oscillation maximum (*max*) and minimum (*min*) for $[Ca_i^{2+}]$ are plotted as functions of the Ca^{2+} influx rate, j_{in}. Parameters are for the large internal store given in Table 3. The amplitude of the oscillations is nearly independent of j_{in}.

notable. First, there are both upper and lower threshold values of j_{in} above and below which oscillations do not occur. Second, in the range of values of j_{in} that corresponds to oscillations, the amplitude is almost constant. Third, the frequency of the oscillations increases as j_{in} increases (from 0.18 min^{-1} at j_{in} = 0.5 $\mu M\ s^{-1}$ to 0.50 min^{-1} at j_{in} = 1.3 $\mu M\ s^{-1}$). These results are in general agreement with those reported by Friel and Tsien (1992). In their experiments initiation of oscillations in the bullfrog sympathetic neuron requires depolarization of sufficient magnitude. Nonetheless they found little change in amplitude but a decrease in frequency when external Ca^{2+} was lowered from 1.0 to 0.5 mM. CICR is the only destabilizing part of the simplified model. As in the model of Friel (1995), it is CICR that is responsible for the oscillations.

The simplified model is easy to analyze and provides an explanation for the occurrence of the high-amplitude oscillations when the internal stores are large. Figure 9 gives a geometric or phase-plane representation (Edelstein-Keshet, 1988) of the simplified equations by plotting the curves on which the time derivatives of $[Ca_i^{2+}]$ and C_o vanish. We obtain these so-called nullclines by setting the right-hand sides of Eqs. 10 and 11 equal to zero. Analytical expressions are easily obtained for the $[Ca_i^{2+}]$ nullcline:

$$C_o = (1 + c_1)([Ca_i^{2+}]) + c_1 \frac{(-j_{in} + j_{out}([Ca_i^{2+}]) + j_{pump}([Ca_i^{2+}]))}{(v_1 P_o^{slow}([Ca_i^{2+}]) + v_2)}, \quad (13)$$

and for the C_o nullcline:

$$C_o = K_{out}\left(\frac{j_{in}/v_{out}}{1 - j_{in}/v_{out}}\right)^{0.5}, \quad (14)$$

where $j_{pump}([Ca_i^{2+}])$ and $j_{out}([Ca_i^{2+}])$ represent the expressions for the SERCA and the PMCA pumps in Eq. 10.

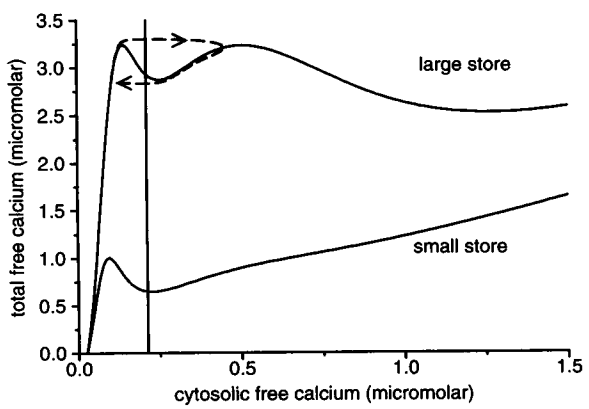

FIGURE 9 Nullclines of the simplified open-cell model for the large and the small stores. The vertical nullcline is for the C_o equation (cf. Eq. 14); the remaining curves are nullclines for the $[Ca_i^{2+}]$ equation (cf. Eq. 13). For these parameters (the same as for Fig. 8, with j_{in} = 1.0 $\mu M\ s^{-1}$), the intersection of the nullclines is an unstable steady state. (— — — —) The oscillatory trajectory surrounding the unstable state, with arrows showing direction of change in time.

These are graphed in Fig. 9. Notice that the vertical line is the C_o nullcline and that the Ca^{2+} nullcline for large stores has two maxima and for small stores has only one maximum. The intersection of the $[Ca_i^{2+}]$ and C_o nullclines determines the steady states (where both $d[Ca_i^{2+}]/dt$ and dC_o/dt vanish).

For the parameter values in Table 3 the steady state occurs in the region of negative slope of the Ca^{2+} nullcline (see Fig. 9), the steady state is unstable, and oscillations occur. Superimposed upon the large-store nullcline is the closed trajectory (*dashed curve with arrows*), corresponding to the oscillation in Fig. 8 at j_{in} = 1.0 $\mu M\ s^{-1}$. Notice that the minimum of the $[Ca_i^{2+}]$ oscillation occurs on the slow, left-hand branch of the $[Ca_i^{2+}]$ nullcline, whereas the peak of the spike occurs on the fast, right-hand branch. These two branches represent states dominated by the closed (*left*) and open (*right*) states of the RyR. The oscillations, which closely follow the two nullclines, are typical of relaxation oscillations for N-shaped nullclines (Edelstein-Keshet, 1988).

Although all the rates in the simplified model have an influence on the shape of the $[Ca_i^{2+}]$ nullcline, the rates of the SERCA pump and RyR (v_3 and v_1, respectively) have a more significant effect than j_{in}, v_{out}, and v_2 (leak) because of their relative sizes. Moreover, the only rates that the C_o nullcline depends on are j_{in} and v_{out} (cf. Eq. 14). Increasing j_{in} (or decreasing v_{out}) moves the vertical C_o nullcline to the right. Because doing this has little effect on the $[Ca_i^{2+}]$ nullcline, there is little change in the amplitude of the oscillation as long as the two nullclines intersect as shown in Fig. 9. This explains the lack of influence of j_{in} on the amplitude of the oscillation in Fig. 8. Similarly, the increase in frequency as j_{in} increases in Fig. 8 is explained by the steady states' moving away from the slow, baseline branch of the $[Ca_i^{2+}]$ nullcline. Thus both effects are a consequence of the large relative sizes of the rates of influx and efflux from the internal stores.

The appearance of large-amplitude oscillations in $[Ca_i^{2+}]$ for large internal stores, but not for small stores, can also be understood from Fig. 9. The double maxima in the nullcline for large stores provide two mechanisms for large-amplitude oscillations. First, for certain parameters the maximum on the left can exceed that on the right (e.g., v_2 = 0.4 s^{-1}). In that case the trajectory is no longer "trapped" in the leftmost well, as it is in Fig. 9, and the maximum is determined by the far-right branch of the $[Ca_i^{2+}]$ nullcline. This results in a sudden transition in amplitude by a factor of ~5 when v_2 falls just below 0.462 s^{-1}. Second, parameters exist (i.e., j_{in} = 6.0 $\mu M\ s^{-1}$) for which the C_o nullcline intersects the negative slope of the $[Ca_i^{2+}]$ nullcline to the right of the second maximum. This also produces a large amplitude oscillation. Small stores tend to reduce the rightmost maximum or to eliminate it entirely, as is the case in Fig. 9, so abrupt changes in amplitude are not observed. According to Eq. 13 the $[Ca_i^{2+}]$ nullcline for small stores ($c_1 \leq 0.05$) is dominated by the first, linear term, which

suppresses the nonlinear contribution to the nullcline from the SERCA pump and the RyR.

It is not accidental that the $[Ca_i^{2+}]$ nullclines in Fig. 9 resemble the shapes of the steady-state curves in Figs. 3 and 4. In fact, if the parameters used in Table 3 are used to calculate the steady-state Ca^{2+} curve in Fig. 3, then the only difference from Fig. 9 is due to the external influx and efflux terms in Eq. 10, which we have noted are minor. The most significant difference between the open- and closed-cell models is that the total free-calcium concentration varies in the open cell. For values of j_{in} in an appropriate range this allows the cell to oscillate between the states of low and high $[Ca_i^{2+}]$ that coexist in the closed cell (cf. Fig. 3). In other words, it is the phenomenon of bistability found in the closed model, not adaptation, that is the cause of the oscillations in the open cell. In an open cell the possibility of refilling the internal stores by means of influx causes a transition between states of high and low $[Ca_i^{2+}]$ that would coexist stably in a closed cell.

DISCUSSION

It has been suggested that adaptation might be an essential feature of Ca^{2+} oscillations and waves in cells that express the RyR (Tang and Othmer, 1994; Sachs et al., 1995). This idea is based partly on the analogy of adaptation to slow Ca^{2+}-dependent inactivation of the IP_3R, which is believed to be a key element of IICR-based Ca^{2+} oscillations and waves (Atri et al., 1993; Jafri and Keizer, 1994, 1995). Moreover, several groups of researchers (Cheng et al., 1995; Sachs et al., 1995) have suggested mechanisms of adaptation in which binding of $[Ca_i^{2+}]$ to the RyR is necessary for adaptation to occur, as it seems to be for the IP_3R, whereas Tang and Othmer (1994) have translated an early model of Fabiato for Ca^{2+} release in cardiac muscle, using Ca^{2+}-dependent inactivation of the RyR. In contrast to experiment (Chu et al., 1993; Györke and Fill, 1993), that model gives rise to a bell-shaped plateau curve for the open probability with a maximum below 1.0 μM, similar to that used in explanations of oscillations that are due to the IP_3R (De Young and Keizer, 1992). Indeed, that model predicts large amplitude oscillations with a period of several seconds determined by the rate of adaptation, again in analogy to what is found for the IP_3R (Keizer et al., 1995).

Our calculations, which are based on the model of RyR adaptation described above, lead to different conclusions about the role of adaptation in Ca^{2+} oscillations. In our closed-cell model we have found parameter ranges that support fast adaptation-dependent oscillations. However, they are generally associated with stable steady states at unphysiologically high values of $[Ca_i^{2+}]$. Furthermore, when realistic values of Ca^{2+} influx and efflux from the external medium are added to the calculations, high-frequency oscillations associated with the rate of adaptation are not observed. Instead, in the open-cell model we find low-frequency oscillations in Ca^{2+} that involve partial emptying and refilling of the internal stores. This is identical to what is found in a model of IICR (see Fig. 10 of Li et al., 1995) at saturating concentrations of IP_3 (where IICR and CICR become equivalent). Indeed, in both that model and the open-cell RyR model presented here the rate of refilling of the stores determines the oscillation period.

Analysis of the open probability for the open-cell model reveals that adaptation plays a role in the decline of the spike. In particular, the upstroke is dominated by the peak open probability, whereas the downstroke occurs primarily on the plateau (cf. Fig. 7). The fact that adaptation is not a determining feature of the oscillations is supported by the fact that increasing or decreasing the rate of adaptation does not halt the oscillations. Removing the external flux, however, does. Thus we conclude that the role of adaptation is to help to attenuate CICR by means of the transition from the peak to the plateau but otherwise is not essential for the oscillations.

Valdivia et al. (1995) have reported that raising the concentration of Mg^{2+} to physiological values increases the rate of adaptation by more than an order of magnitude. This suggests a simplification of the open-cell model in which adaptation is relatively fast, with the open probability of the RyR following the plateau curve as $[Ca_i^{2+}]$ changes. Analysis of the simplified model shows that the rates of influx and efflux do not significantly alter the balance equation for $[Ca_i^{2+}]$. On the contrary, it is CICR, not adaptation, that provides the dynamical instability for the open-cell oscillations that periodically empty and refill the internal stores. These oscillations have their origin in coexisting states of high and low $[Ca_i^{2+}]$ found in closed cells.

The simplified model is similar to that used by Friel (1995) to analyze caffeine-sensitive oscillations in the bullfrog sympathetic neuron. The chief differences are that Friel uses linear, phenomenological expressions to describe influx into the store as well as influx and efflux via the plasma membrane. Otherwise both predict oscillations that involve rapid depletion by means of CICR followed by slower refilling of the internal store. Analysis of our simplified model shows that the physical size of the store is important, with larger stores being capable of large amplitude oscillations because of the increased influence of CICR and the SERCA pumps. Our calculations explain the lack of change of amplitude of the oscillations when the influx rate is altered experimentally (Friel and Tsien, 1992) by the weak role of the plasma membrane in the overall Ca^{2+} balance for these cells. Similarly, the increase in frequency of the oscillations when the influx rate is increased is explained by the increase in rate at which the stores refill.

So is adaptation essential for Ca^{2+} oscillations when store release is controlled by the RyR? In our view, probably not. Adaptation is probably too fast in vivo to provide the necessary slow negative feedback to produce oscillations. Instead, our simulations suggest that it is the bistable behavior of $[Ca_i^{2+}]$ in closed cells coupled to the slow influx of Ca^{2+} from the external medium that is responsible. In this mechanism, CICR leads to a rapid release of Ca^{2+} from

stores, which is partially pumped out of the cell and partially pumped back into the stores. This is followed by a slow refilling of the stores until the driving force for the RyR increases to the point where CICR again develops into a regenerative mechanism for release.

Recent observations of so-called "calcium sparks" in cardiac myocytes (Cheng et al., 1993) suggests that the stochastic properties of the RyR underlie Ca^{2+} waves in these cells (Cheng et al., 1996). We are currently using an extension of our kinetic model of the cardiac RyR to describe the dynamics of calcium sparks in vivo. We believe that this type of modeling will help to provide insight into oscillatory wave propagation through CICR in myocytes and other cells that depend on RyR-mediated Ca^{2+} release.

This study was supported in part by funds from National Science Foundation grants BIR 9214381 and BIR 9300799, National Institutes of Health grant R01 RR10081-01A1, and the Agricultural Experiment Station of the University of California, Davis. A summary of this study appears in the undergraduate honors thesis of L. Levine.

APPENDIX A: PEAK AND PLATEAU DEPENDENCE ON $[Ca^{2+}]$

Analytical expressions for the peak and plateau values of P_O are easily derived for the kinetic equations (1–4). Inasmuch as kinetic steps *a* and *b* in Fig. 1 are several orders of magnitude faster than step *c*, we can approximate the peak value of P_O by the quasi-equilibrium value of P_O obtained by ignoring the slow rate of step *c*. Taking $n = 4$ and $m = 3$ (see Table 1) gives

$$P_O^{peak}([Ca_i^{2+}]) = \frac{w^e(0.1\ \mu M)(1 + ([Ca_i^{2+}]/K_b)^3)}{1 + (K_a/[Ca_i^{2+}])^4 + ([Ca_i^{2+}]/K_b)^3}, \quad (15)$$

where w^e (0.1 μM) is the equilibrium value of $1 - P_{C_2}$ evaluated at the initial value of $[Ca_i^{2+}] = 0.1\ \mu M$. For the parameters in Table 1 w^e (0.1 μM) = 0.963, which determines the maximum value of P_O in Fig. 2 *C*. The three dissociation constants, K_i, in Eq. 15 are $K_a^4 = k_a^-/k_a^+$, $K_b^3 = k_b^-/k_b^+$, and $K_c = k_c^-/k_c^+$.

The rate of rise to the peak value of P_O in Eq. 15 can be obtained from Eqs. 1 and 3 supplemented with the condition that $P_{O_1} = 1 - P_{C_1} + P_{C_2} + P_{O_2}$, with P_{C_2} held constant at its initial value 0.037. For the parameter values given in the legend of Fig. 2 and a final value of $[Ca_i^{2+}] = 0.9\ \mu M$ we obtain a single relaxation time of 1.1 ms, which compares with the experimental value of 1.1 ± 0.3 ms. This relaxation time increases by a factor of ~4 when $[Ca_i^{2+}] = 0.5\ \mu M$.

The plateau value of P_O in the model is the equilibrium value of $P_{O_1} + P_{O_2}$ determined by solution of Eqs. 1–4 when the left-hand sides vanish. This value of P_O is

$$P_O^{plateau}([Ca_i^{2+}]) = \frac{1 + ([Ca_i^{2+}]/K_b)^3}{1 + (K_a/[Ca_i^{2+}])^4 + ([Ca_i^{2+}]/K_b)^3 + 1/K_c}. \quad (16)$$

APPENDIX B: RELAXATION TO THE PLATEAU

One can derive the approximate differential equation (6) for the relaxation of $w = 1 - P_{C_2}$ by taking advantage of the rapid equilibration of kinetic steps *a* and *b* compared with *c*. For any instantaneous value P_{C_2} this gives

$$P_{O_1} = \frac{w}{1 + (K_a/[Ca_i^{2+}])^4 + ([Ca_i^{2+}]/K_b)^3}, \quad (17)$$

where the facts that $w = 1 - P_{C_2} = P_{C_1} + P_{O_1} + P_{O_2}$ were also used. The comparable expression for P_{O_2} combined with Eq. 17 gives rise to the expression for P_O on the slower time scale (cf. Eq. 15):

$$P_O^{slow} = \frac{w(1 + ([Ca_i^{2+}]/K_b)^3)}{1 + (K_a/[Ca_i^{2+}])^4 + ([Ca_i^{2+}]/K_b)^3}. \quad (18)$$

Substituting Eq. 17 and the definition of w into Eq. 4 gives

$$dw/dt = -\frac{k_c^+}{1 + (K_a/[Ca_i^{2+}])^4 + ([Ca_i^{2+}]/K_b)^3} w - k_c^-(w - 1). \quad (19)$$

With a little algebra Eq. 19 is easily rearranged into Eq. 6 with the definitions

$$w^\infty([Ca_i^{2+}]) = \frac{1 + (K_a/[Ca_i^{2+}])^4 + ([Ca_i^{2+}]/K_b)^3}{1 + (1/K_c) + (K_a/[Ca_i^{2+}])^4 + ([Ca_i^{2+}]/K_b)^3}. \quad (20)$$

$$\tau([Ca_i^{2+}]) = w^\infty([Ca_i^{2+}])/k_c^-. \quad (21)$$

REFERENCES

Alberts, B., D. Bray, J. Lewis, M. Raff, K. Roberts, and J. D. Watson. 1989. Molecular Biology of the Cell, 2nd ed. (Garland, New York).

Atri, A., J. Amundson, D. Clapham, and J. Sneyd. 1993. A single-pool model for intracellular calcium oscillations and waves in the *Xenopus laevis* oocyte. *Biophys. J.* 65:1727–1739.

Berridge, M. J. 1993. Inositol trisphosphate and calcium signalling. *Nature (London)*. 361:315–325.

Berridge, M., and A. Galione. 1988. Cytosolic calcium oscillators. *FASEB J.* 2:3074–3084.

Bezprozvanny, I., J. Watras, and B. E. Ehrlich. 1991. Bell-shaped calcium response curves of Ins(1,4,5)P_3- and calcium-gated channels from endoplasmic reticulum of cerebellum. *Nature (London)*. 351:751–754.

Carafoli, E. 1994. Biogenesis: plasma membrane calcium ATPase, 15 years of work on the purified enzyme. *FASEB J.* 8:993–1002.

Cheng, H., M. Fill, H. Valdivia, and W. J. Lederer. 1995. Models of Ca^{2+} release channel adaptation. *Science.* 267:2009–2010.

Cheng, H., W. J. Lederer, and M. B. Cannell. 1993. Calcium sparks: elementary events underlying excitation-contraction coupling in heart muscle. *Science.* 262:740–744.

Cheng, H., M. R. Lederer, W. J. Lederer, and M. B. Cannell. 1996. Calcium sparks and $[Ca_i^{2+}]$ waves in cardiac myocytes. *Am. J. Physiol. (Cell Physiol. 39).* 270:C148–C159.

Chu, A., M. Fill, E. Sefani, and M. L. Entman. 1993. Cytoplasmic Ca^{2+} does not inhibit the cardiac muscle sarcoplasmic reticulum ryanodine receptor Ca^{2+} channel, although Ca^{2+}-induced inactivation of Ca^{2+} release is observed in native vesicles. *J. Membr. Biol.* 135:49–59.

De Young, G., and J. Keizer. 1992. A single-pool inositol 1,4,5-trisphosphate-receptor-based model for agonist-stimulated oscillations in Ca^{2+} concentration. *Proc. Natl. Acad. Sci. USA.* 89:9895–9899.

Edelstein-Keshet, L. 1988. Mathematical Models in Biology. (Random House, New York).

Ermentrout, B. 1995. Xppauto—the differential equation tool (bard@mthbard.math.pitt.edu).

Finch, E. A., T. J. Turner, and S. M. Goldin. 1991. Calcium as a coagonist of inositol 1,4,5-trisphosphate induced calcium release. Science 252: 443–446.

Friel, D. 1995. $[Ca_i^{2+}]$ oscillations in sympathetic neurons: An experimental test of a theoretical model. *Biophys. J.* 68:1752–1766.

Friel, D., and R. W. Tsien. 1992. Phase-dependent contributions from Ca^{2+} entry and Ca^{2+} oscillations in bullfrog sympathetic neurons. *Neuron.* 8:1109–1125.

Györke, S., and M. Fill. 1993. Ryanodine receptor adaptation: control mechanism of Ca^{2+}-induced Ca^{2+} release in heart. *Science.* 260:807–809.

Györke, S., and M. Fill. 1994. Ca^{2+}-induced Ca^{2+} release in response to flash photolysis. *Science.* 263:987–988.

Györke, S., P. Vélez, B. Suárez-Isla, and M. Fill. 1994. Activation of single cardiac and skeletal ryanodine receptor channels by flash photolysis of caged Ca^{2+}. *Biophys. J.* 66:1879–1886.

Hille, B. 1992. Ionic Channels of Excitable Membranes, 2nd ed. (Sinauer Associates, Sunderland, MA).

Hofer, A. M., and T. E. Machen. 1994. Direct measurement of free Ca in organelles of gastric epithelial cells. *Am. J. Physiol.* (*Gastrointest. Liver Physiol.*) 267:G442–G451.

Iino, M. 1990. Biphasic Ca^{2+}-dependence of inositol 1,4,5-trisphosphate-induced Ca^{2+} release in smooth muscle cells of the guinea pig *Taenia caeci*. *J. Gen. Physiol.* 95:1103–1122.

Iino, M., and M. Tsukioka. 1994. Feedback control of inositol trisphosphate signaling by calcium. *Mol. Cell. Endocrinol.* 98:141–146.

Jafri, M. S., and J. Keizer. 1994. Diffusion of inositol 1,4,5-trisphosphate but not Ca^{2+} is necessary for a class of inositol 1,4,5-trisphosphate-induced Ca^{2+} waves. *Proc. Natl. Acad. Sci. USA.* 91:9485–9489.

Jafri, M. S., and J. Keizer. 1995. On the roles of Ca^{2+} diffusion, Ca^{2+} buffers, and the endoplasmic reticulum in IP_3-induced Ca^{2+} waves. *Biophys. J.* 69:2139–2153.

Keizer, J., Y.-X. Li, S. Stojilović, and J. Rinzel. 1995. $IP_3$3-induced Ca^{2+} excitability of the endoplasmic reticulum. *Mol. Biol. Cell.* 6:945–951.

Laver, D. R., L. D. Roden, G. P. Ahern, K. R. Eager, P. R. Junankar, and A. F. Dulhunty. 1995. Cytoplasmic Ca^{2+} inhibits the ryanodine receptor from cardiac muscle. *J. Membr. Biol.* 147:7–22.

Li, Y.-X., J. Keizer, S. Stojilković, and J. Rinzel. 1995. Ca^{2+} excitability of the ER membrane: an explanation for IP_3-induced Ca^{2+} oscillations. *Am. J. Physiol.* (*Cell Physiol. 38*) 269:C1079–C1092.

Louis, C. F. 1994. Caged calcium and the ryanodine receptor. *Biophys. J.* 66:1739–1741.

Lytton, J., M. Westlin, S. E. Burk, G. E. Shull, and D. H. MacLennan. 1992. Functional comparisons between isoforms of the sarcoplasmic or endoplasmic reticulum family of calcium pumps. *J. Biol. Chem.* 267: 14,483–14,489.

Ogawa, Y. 1994. Role of ryanodine receptors. *Crit. Rev. Biochem. Mol. Biol.* 29:229–274.

Sachs, F., F. Qin, and P. Palade. 1995. Models of Ca^{2+} release channel adaptation. *Science.* 267:2010–2011.

Scharff, O., and B. Foder. 1993. Regulation of cytosolic calcium in blood cells. *Physiol. Rev.* 73:547–582.

Tang, Y., and H. Othmer. 1994. A model of calcium dynamics in cardiac myocytes based on the kinetics of ryanodine-sensitive calcium stores. *Biophys. J.* 67:2223–2235.

Tepikin, A. V., S. G. Voronia, D. V. Gallacher, and O. H. Petersen. 1992. Pulsitile Ca^{2+} extrusion from single pancreatic acinar cells during receptor-activated cytosolic Ca^{2+} spiking. *J. Biol. Chem.* 267: 14,073–14,076.

Tse, A., F. W. Tse, and B. Hille. 1994a. Calcium homeostasis in identified rat gonadotrophs. *J. Physiol.* 477:511–525.

Tse, A., F. W. Tse, and B. Hille. 1994b. Cyclic Ca^{2+} changes in intracellular stores of gonadotrophs during gonadotropin-releasing hormone-stimulated Ca^{2+} oscillations. *Proc. Natl. Acad. Sci. USA.* 91: 9750–9754.

Valdivia, H., J. H. Kaplan, G. C. R. Ellis-Davies, and W. J. Lederer. 1995. Rapid activation of cardiac ryanodine receptors: modulation by Mg^{2+} and phosphorylation. *Science.* 267:1997–2000.